

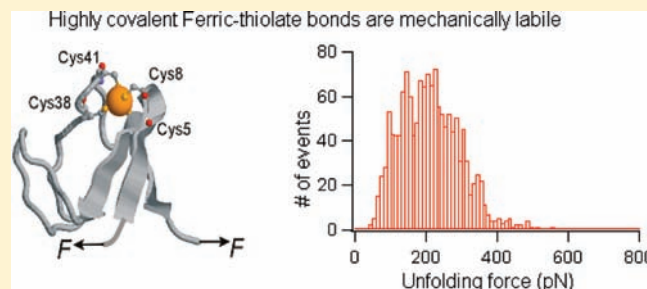
Highly Covalent Ferric–Thiolate Bonds Exhibit Surprisingly Low Mechanical Stability

Peng Zheng and Hongbin Li*

Department of Chemistry, University of British Columbia, Vancouver, BC V6T 1Z1, Canada

Supporting Information

ABSTRACT: Depending on their nature, different chemical bonds show vastly different stability with covalent bonds being the most stable ones that rupture at forces above nanonewton. Studies have revealed that ferric–thiolate bonds are highly covalent and are conceived to be of high mechanical stability. Here, we used single molecule force spectroscopy techniques to directly determine the mechanical strength of such highly covalent ferric–thiolate bonds in rubredoxin. We observed that the ferric–thiolate bond ruptures at surprisingly low forces of ~ 200 pN, significantly lower than that of typical covalent bonds, such as C–Si, S–S, and Au–thiolate bonds, which typically ruptures at >1.5 nN. And the mechanical strength of Fe–thiolate bonds is observed to correlate with the covalency of the bonds. Our results indicated that highly covalent Fe–thiolate bonds are mechanically labile and display features that clearly distinguish themselves from typical covalent bonds. Our study not only opens new avenues to investigating this important class of chemical bonds, but may also shed new lights on our understanding of the chemical nature of these metal thiolate bonds.



INTRODUCTION

Chemical bonding, which describes the degree of interactions between atoms, is a fundamental concept in chemistry. Depending on their nature, different chemical bonds display vastly different strength and stability with covalent bonds being the most stable ones. Single molecule force spectroscopy studies^{1,2} have shown that the mechanical stability, defined as the most probable force at which the bond ruptures, of chemical bonds also follow this hierarchy: the rupture force of noncovalent bonds such as hydrogen bonds ranges from a few piconewton to a few tens of piconewtons, while covalent bonds rupture at forces that are orders of magnitude higher, ranging from 1.4 to 3 nN.^{1–7} Mechanical strength of chemical bonds provides new information about chemical bonds that is complementary to the classical thermodynamic one.²

Fe–S bonds are ubiquitous in nature and an essential component of a myriad of proteins.⁸ These bonds are highly covalent,^{9,10} making Fe–S-containing proteins suitable electron transfer proteins^{8,11,12} as well as providing structural roles to facilitate protein folding and maintain their overall three-dimensional structures.¹² Because of their highly covalent nature, it is conceived that these Fe–S bonds are mechanically stable and should be of high mechanical stability. However, no experimental study is available. To understand the mechanical nature of such highly covalent Fe–S bonds, here we combined single molecule atomic force microscopy (AFM) and protein engineering techniques to carry out the first direct experimental measurement of the mechanical strength of highly covalent ferric–thiolate bonds in rubredoxins. For this purpose, rubredoxin from *Pyrococcus*

furiosus (RD) was used as a model system. Rubredoxin is the simplest iron–sulfur protein, which consists of one iron atom bound by four cysteinyl sulfur atoms in a pseudo-tetrahedral fashion (Figure 1A).^{13,14} On the basis of their bond length, the four Fe(III)–thiolate bonds can be categorized into two groups: Fe–S8 and Fe–S38 belong to one group with a bond length of ~ 2.31 Å, while Fe–S41 and Fe–S5 belong to the other group displaying a shorter bond length of ~ 2.25 Å. Fe(III)–thiolate bonds are highly covalent with a total covalency of $\sim 130\%$ measured by sulfur K-Edge X-ray absorption spectroscopy (S K-edge XAS).¹⁵ Upon reduction, these Fe–S bonds lengthen by an average of 0.033 Å accompanied by a significant reduction in their covalency.^{16,17} The four coordinating cysteine residues are grouped into two CXXC chelating motifs (C5XXC8 and C38XXC41) and are highly conserved in different types of rubredoxins.^{13,17} Thus, rubredoxins provide an ideal model system to study mechanical strength of highly covalent Fe–S bonds.

AFM-based single molecule force spectroscopy technique has evolved into a powerful tool to investigate the mechanical activation (bond rupture) of chemical bonds, ranging from noncovalent bonds (such as hydrogen bonds) to covalent bonds (such as C–Si bonds), and the influence of stretching force on chemical reactions.^{1,2,18–20} Here, we used single molecule AFM to directly measure the mechanical bond strength of Fe–thiolate bonds in rubredoxin and investigate the nature of their mechanical activation.

Received: January 24, 2011

Published: April 08, 2011

MATERIALS AND METHODS

Protein Engineering. The plasmid encoding the gene of *P. furiosus* rubredoxin (RD) is a generous gift from Dr. Eidsness. The gene of protein chimera Cys-RD-GB1-Cys was constructed in expression vector pQE80L using well-established standard molecular biology techniques,²¹ where GB1 (the B1 IgG binding domain of protein G from *Streptococcus*) is used as a fingerprint domain for single molecule AFM experiments. Cys-RD-GB1-Cys was overexpressed in *Escherichia coli* strain DH5 α and purified by Co²⁺-affinity chromatography using TALON resins (Clontech). The protein was kept in Tris buffer in pH 7.4 at a concentration of ~ 2 mg/mL. Cys-cpRD-GB1-Cys was constructed in a similar fashion. Histidine mutants of rubredoxin were generated via standard site-directed mutagenesis methods using the RD gene as the template. Pseudo-apo-RD (apoRD), which contains four mutations Cys5Lys, Cys8Thr, Cys38Ala and Cys41Thr,²² was generated via the megaprimer approach using the wt-RD as the template.

Since Zn-RD and Fe-RD are co-expressed in *E. coli*,¹³ we used ion-exchange chromatography to produce pure Fe(III)-RD-GB1 proteins. First, the protein chimera RD-GB1 was concentrated and buffer exchanged into a 10 mM Tris buffer at pH 8.5 using a 9K MWCO pierce concentrator (Thermo Scientific). The Fe and Zn form RD were separated using Mono-Q 5/50GL anion exchange column (GE Healthcare), and eluted using a linear gradient elution (0–300 mM NaCl in 10 mM Tris buffer with 1 mM TCEP at pH 8.5) in AKTA FPLC system (GE Healthcare) at a flow rate of 2 mL/min. The Fe-RD-GB1 was eluted first at around 100 mM NaCl (Supporting Information, Figure S1A). The purity of Fe-form RD was confirmed by UV–Vis Absorption Spectroscopy based on its characteristic absorbance at 494 nm (Supporting Information, Figure S1B). Using the extinction coefficient of 9.22 mM⁻¹ cm⁻¹ at 494 nm, the concentration of Fe(III)-RD was calculated, and the overall protein concentration was obtained by measuring the absorbance at 280 nm.¹³ The purity of Fe(III)-RD was estimated to be >90% after 2 to 3 times ion-exchange chromatography purification. The Fe-form of the rubredoxin mutants were purified using the same method.

Engineering Polyproteins for Single Molecule AFM Experiments. The polyprotein gene (I27-apoRD)₄ was engineered using the well-established stepwise DNA-concatamerization method based on the identity of the sticky ends generated by *Bam*HI and *Bgl*III restriction digestion.²¹ The polyprotein (I27-apoRD)₄ was overexpressed in DH5 α and purified by Co²⁺-affinity chromatography using TALON resins.

Since Zn-RD and Fe-RD are co-expressed in *E. coli*,¹³ the conventional method for polyprotein construction cannot be used to construct polyproteins of rubredoxin, as it will lead to the production of mixed metal-containing rubredoxin.¹³ To overcome this hurdle, we developed a novel method based on maleimide-thiol coupling chemistry to construct polyprotein chimera (Fe(III)-Rd-GB1)_n, in which rubredoxin exists solely as Fe(III)-RD (Supporting Information, Figure S1C). In a typical reaction, 40 μ L of 10 mM BM(PEO)₃ (1,8-bis-maleimido-(PEO)₃, Molecular Biosciences) solution was added to 1 mL of Fe(III)-RD-GB1 solution (at a concentration of 2 mg/mL in Tris buffer under pH 7.4), which was purified via ion-exchange chromatography to remove Zn-RD, at a molar ratio of 1 to 1. The solution was incubated for polymerization for two hours, and the protein solution was used directly in AFM experiments.

Single-Molecule AFM Experiments. Single-molecule AFM experiments were carried out on a custom-built AFM as described.²³ Each individual cantilever (Si₃N₄ cantilevers from Bruker Corp.) was calibrated in solution using the equipartition theorem before each experiment to obtain the spring constant (typically around 40 pN/nm). All experiments were done at room temperature in Tris buffer at pH 7.4 at a pulling speed of 400 nm/s unless otherwise indicated.

For experiments on Fe(II)-RD, after the (Fe(III)-RD-GB1)_n protein was absorbed onto the glass coverslip, 10 μ L of 200 mM dithiothreitol (DTT) was added to the solution. After 15 min of incubation, the protein

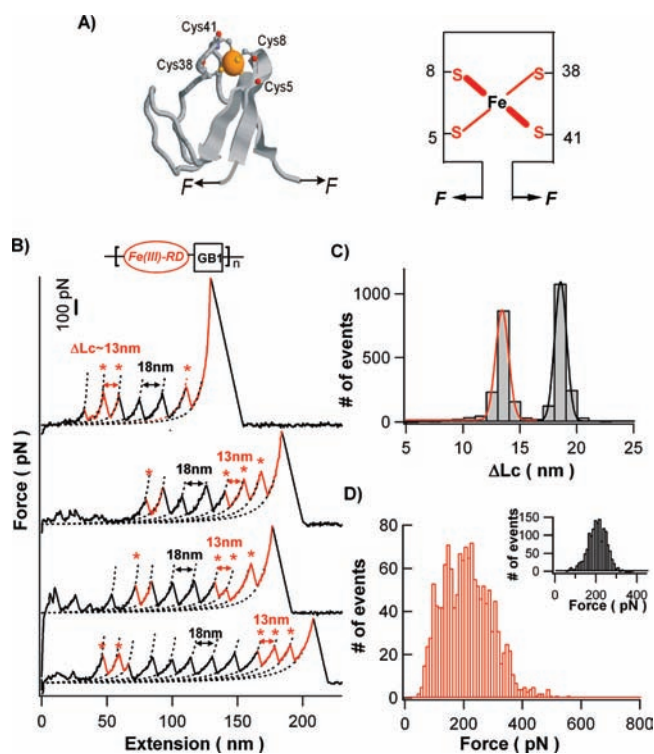


Figure 1. Mechanical unfolding experiments on polyprotein (Fe(III)-RD-GB1)_n revealed that the Fe(III)–S₄ center ruptures at low forces. (A) Three-dimensional structure of Fe(III)-ppRD (PDB code: 1brf). The iron is coordinated by four cysteinyl sulfur atoms arranged in a pseudo-tetrahedral environment. The four cysteines belong to two groups of CXXC chelating motif. The iron and coordinating cysteine are highlighted in ball and stick model. Right panel schematically shows the pulling geometry of Fe(III)-RD in single-molecule AFM experiments. Thicker red lines indicate the shorter Fe(III)–thiolate bonds (Fe–S8 and Fe–S41) and thinner red lines indicate the longer Fe(III)–thiolate bonds (Fe–S5 and Fe–S38). (B) Typical force–extension curves of (Fe(III)-RD-GB1)_n. The force–extension curves are characterized by two groups of unfolding events with different contour length increments. The mechanical unfolding events of GB1 (colored in black) are characterized by Δ Lc of ~ 18 nm. The unfolding events of Δ Lc of ~ 13 nm (colored in red) are attributed to the unfolding of Fe(III)-RD domains in the polyprotein. Dotted lines correspond to the WLC fits to the experimental data. The top panel shows the schematics of the polyprotein (Fe(III)-RD-GB1)_n. (C and D) Mechanical unfolding signatures of Fe(III)-RD. The contour length increment Δ Lc of Fe(III)-RD shows a narrow distribution (shown in C) with an average of 12.6 ± 1.3 nm ($n = 1421$), which agrees well with the contour length increment of rupturing the Fe(III)–S₄ center and extension of the polypeptide from residues 5–41. The Δ Lc histogram for GB1 is shown in black in panel C with an average of 18.2 ± 0.8 nm ($n = 1534$). Solid lines in panel C are Gaussian fits to the experimental data. The histogram of the rupture forces of Fe(III)–S₄ (shown in panel D) is characterized by a very broad distribution, with an average of 211 ± 86 pN ($n = 1421$). For comparison, the unfolding force histogram of GB1 is shown in the inset of panel D. The pulling speed was 400 nm/s.

was subject to AFM experiments. To ensure the reducing environment, the same amount of DTT solution was added every hour thereafter.

RESULTS

In single-molecule AFM experiments, the construction of polyproteins or polyprotein chimera is necessary for identifying

mechanical unfolding signatures of proteins in an unambiguous fashion.²¹ Since Zn-substituted RD and Fe-RD are co-expressed in *E. coli*, the conventional DNA-concatamerization method for polyprotein construction will lead to the production of mixed metal-containing rubredoxin.¹³ To overcome this hurdle, we developed a novel method based on maleimide–thiol coupling chemistry to construct polyprotein chimera (Fe(III)-Rd-GB1)_n, in which rubredoxin exists solely as Fe(III)-RD (Supporting Information, Figure S1). In (Fe(III)-Rd-GB1)_n, Fe(III)-RD alternates with the well-characterized GB1 domain, which was used as the internal force calibrator and fingerprint for identifying single molecule stretching events for (Fe(III)-RD-GB1)_n.^{23,24}

FeS₄ Center in Rubredoxin Ruptures at ~200 pN. Stretching polyprotein (RD-GB1)_n results in force–extension curves of characteristic sawtooth-like appearance (Figure 1B), in which individual force peaks correspond to the mechanical unfolding of individual domains and the last peak corresponds to the stretching of the fully unfolded polypeptide chain and its subsequent detachment from either the AFM tip or glass substrate. The force–extension curves of (RD-GB1)_n are characterized by two populations of unfolding force peaks. Fitting the Worm-like chain model of polymer elasticity²⁵ to consecutive force peaks revealed that one group of force peaks displayed contour length increments ΔLc of 18.2 ± 0.8 nm (colored in black, $n = 1534$), which is the unfolding signatures of the well-characterized GB1 domains,²³ while the other group (colored in red) showed ΔLc of 12.6 ± 1.3 nm (average \pm standard deviation, $n = 1421$) (Figure 1C). Since rubredoxin alternates with GB1 in (RD-GB1)_n, the unfolding events of ΔLc of ~ 13 nm can thus be attributed to the mechanical unfolding of Fe(III)-RD. Single-molecule AFM experiments on the polyprotein (I27-RD)_n, where the I27 domain from the muscle protein titin was used as a fingerprint domain, reached the same conclusion that the unfolding events of ΔLc of ~ 13 nm correspond to the mechanical unfolding of Fe(III)-RD (see Figure S2 and Choice of Fingerprint Domain in Supporting Information).

Contour length increment ΔLc upon domain unfolding is an important structural parameter that can provide detailed information about the unfolding mechanism of a protein.²⁰ If the structure of the protein is known, ΔLc can be calculated: $\Delta Lc = Lc(\text{unfolded}) - Lc(\text{folded})$, where $Lc(\text{unfolded})$ is the length of the unfolded and fully extended polypeptide chain and $Lc(\text{folded})$ is the distance between the N- and C-termini in the folded structure. If there is a strong bond (such as a disulfide bond) in the protein structure linking two parts of the protein, ΔLc will be affected, as the sequence between the strong bond will be sequestered and shielded from the stretching force, as demonstrated for the disulfide bond mutants of I27.^{20,26,27} Rubredoxin contains 53 residues. The highly covalent Fe(III)–thiolate bonds could serve as a strong bond such that rubredoxin sequence enclosed in the FeS₄ center (residues 5–41) is sequestered and shielded from the stretching force until the FeS₄ center ruptures. Thus, when the FeS₄ center is intact, rubredoxin can only partially unravel, leading to the unfolding and stretching of the polypeptide sequence from residues 1 to 5 and 41 to 53. Such a partial unfolding would result in unfolding events of ΔLc of 5.3 nm ($(5 + 13)\text{aa} \times 0.36 \text{ nm/aa} = 1.2 \text{ nm}$, where 1.2 nm is the distance between the N- and C-termini of rubredoxin). However, we did not observe such unfolding events, suggesting that residues 1 to 5 and 41 to 53 unfold at low forces that are below our AFM detection limit (~ 20 pN). Instead, we observed

unfolding events of ΔLc of ~ 13 nm. A ΔLc of ~ 13 nm corresponds to the exposing of a polypeptide of ~ 36 aa ($13 \text{ nm}/0.36 \text{ nm/aa}$) to a stretching force during the mechanical unraveling of rubredoxin. In rubredoxin, there are only 18 aa (residues 1–5, 41–53) outside the FeS₄ center. During the unfolding of Fe(III)-RD, if Fe–thiolate bonds were not broken, it would be impossible to obtain ΔLc of 13 nm. Therefore, the unfolding of Fe(III)-RD must involve the breaking of the Fe(III)–thiolate bonds. In fact, based on the three-dimensional structure of rubredoxin, it is expected that the unraveling of the FeS₄ center and subsequent unfolding of the remainder of rubredoxin (residues 5 to 41) would result in unfolding events of ΔLc of 12.4 nm ($37\text{aa} \times 0.36 \text{ nm/aa} = 0.9 \text{ nm}$). This expected value is in close agreement with our experimentally determined ΔLc of rubredoxin, strongly indicating that the observed unfolding events of rubredoxin correspond to the rupturing of the FeS₄ center and the subsequent unfolding and extending of rubredoxin.

Thus, the mechanical unfolding of Fe(III)-RD occurs in two steps (Figure S3): the first step is the mechanical unraveling of protein structure outside the FeS₄ center (which occurs at low forces); and the second step is the mechanical rupture of the FeS₄ center followed by the unfolding and extension of the remaining structure (residues 5 to 41), leading to the observed unfolding events of ΔLc of ~ 13 nm. It is important to note that in order to rupture the FeS₄ center, at least two Fe(III)–thiolate bonds from the same side of the FeS₄ center need to be broken (Fe–S5/Fe–S8 or Fe–S38/Fe–S41). However, we do not know exactly how many Fe(III)–thiolate bonds are broken during this mechanical unfolding process and whether Fe(III) is still attached to rubredoxin after the FeS₄ center has been mechanically ruptured. In principle, depending on the number of Fe–S bonds that are broken during unfolding, slightly different ΔLc should be observed (the difference is ~ 1 nm). However, the length resolution of our measurements is not sufficient to allow us to unequivocally determine the number of Fe–thiolate bonds that break during AFM experiments. Further experiments are underway to address this issue and the results will be reported in due time.

Having confirmed that the unfolding events of ΔLc of ~ 13 nm correspond to the mechanical rupture of the FeS₄ center, we then measured the rupture force of the FeS₄ center. Figure 1D shows the rupture force histogram of FeS₄ center at a pulling speed of 400 nm/s. The rupture force showed a very broad distribution from 100 pN to 500 pN, with an average rupture force of 211 ± 86 pN ($n = 1421$). This result suggested that the rupture of the FeS₄ center formed by four highly covalent Fe(III)–thiolate bonds occurred at forces of ~ 200 pN, which are surprisingly low compared with the bond strength of typical covalent bonds.^{1,2}

To ensure that we did not miss unfolding events of rubredoxin occurring at forces that are higher than the detachment force, we measured the ratio of the number of unfolding events for rubredoxin versus GB1. Since GB1 alternates with rubredoxin in the polyprotein, the number of rubredoxin unfolding events should be roughly equal to that for GB1. Indeed, the force–extension curves shown in Figure 1B contained roughly the same number of unfolding events of rubredoxin and GB1. The overall ratio between rubredoxin unfolding events and GB1 unfolding events is 0.93:1, which is close to the theoretical ratio of 1. This result indicated that the rupture force histogram for FeS₄ center genuinely reflected the true mechanical strength of the highly covalent ferric–thiolate bonds. And the broad distribution of the rupture force is clearly beyond the experimental

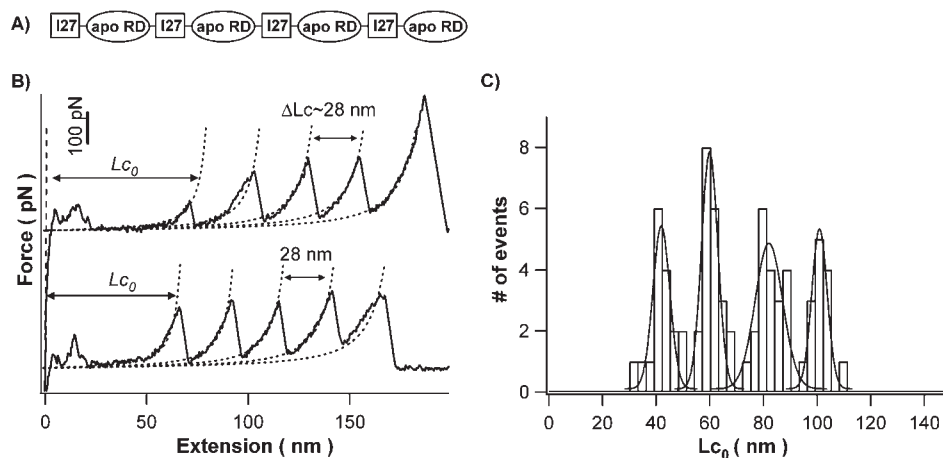


Figure 2. Mechanical unfolding of polyprotein (I27-apoRD)₄ indicates that the unfolding of RD protein structure does not contribute to the rupture force of Fe(III)-RD. (A) A schematic of the polyprotein (I27-apoRD)₄. (B) Typical force–extension curves for (I27-apoRD)₄. The force–extension curves of (I27-apoRD)₄ are characterized by the long featureless spacer followed by the unfolding events of I27 domains, which are characterized by ΔLc of ~ 28 nm. These results suggest that the unfolding of apoRD occurs at forces below the detection limit of our AFM, which is ~ 20 pN. Lc_0 measures the length of the featureless region of the polyprotein, which largely corresponds to the length of unfolded and fully extended apo-RD proteins in the polyprotein construct. (C) Force–extension curves allow accurate measurement of the length of the unfolded and fully extended apo-RD. The distribution of Lc_0 shows four clearly separated peaks ($n = 72$), corresponding to Lc_0 of different length of polyprotein (I27-apoRD)₄ fragments. Gaussian fits give distributions that peak at 41 ± 3.1 , 59 ± 3.0 , 81 ± 5.2 , and 100 ± 2.9 nm, respectively.

errors, and reflected the intrinsic short distance from the bound state to the mechanical dissociation transition state⁴ for ferric–thiolate bonds.

Unfolding of Pseudo Apo-Rubredoxin Shows No Detectable Rupture Force. To confirm that the unfolding of the secondary structures of rubredoxin does not contribute to the rupture force histogram shown in Figure 1D, we measured the unfolding force of a pseudo apo-rubredoxin (apo-RD). This pseudo apo-RD, a computationally designed rubredoxin mutant in which four iron-coordinating cysteines are mutated to alanine, lysine, and threonines, shows the same three-dimensional structure as wild-type Fe(III)-RD but does not have a FeS₄ center.²² If apo-RD is mechanically stable and unfolds in a two-state fashion, the unfolding of apo-RD will result in unfolding events with ΔLc of ~ 17 nm ($53aa \times 0.36$ nm/aa $- 1.2$ nm, where 1.2 is the distance between the N, C-termini of apo-RD). However, this contour length increment is similar to that of GB1, making the identification of apo-RD unfolding events difficult. To avoid this potential complication, we used the well-characterized I27 domain (the 27th Ig domain from the muscle protein titin) as the fingerprint domain,²¹ as the unfolding of I27 leads to ΔLc of ~ 28 nm. We constructed polyprotein (I27-apoRD)₄ for single molecule AFM experiments (Figure 2A). In the vast majority of force–extension curves, we observed that stretching (I27-apoRD)₄ results in sawtooth-like force–extension curves characterized by a long featureless spacer followed by only unfolding events of ΔLc of ~ 28 nm, which correspond to the unfolding of I27 domains (Figure 2B). Hence, the long featureless spacer originates from the unfolding and stretching of the pseudo apo-RD, suggesting that apo-RD is mechanically labile and unfolds at forces that are below the detection limit of our AFM. The distribution of the length of the featureless spacer shows four clearly separated peaks, corresponding to the stretching of different number of I27-apo-RD repeating unit. The measured length is ~ 20 nm per apo-RD, close to the expected contour length of fully extended apo-RD (~ 19 nm). This result

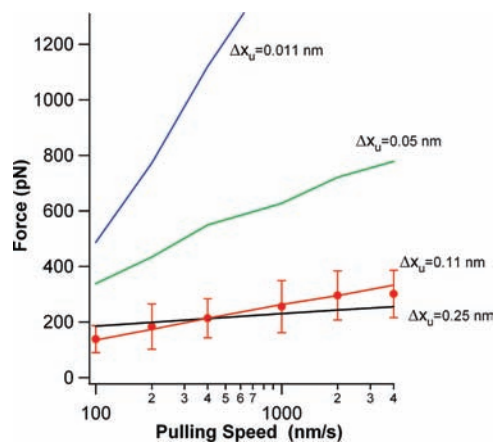


Figure 3. The rupture force of FeS₄ center of rubredoxin depends on the pulling speed. Symbols represent the experimental data, and the red line corresponds to the Monte Carlo simulation using a Δx_u of 0.11 nm and a spontaneous dissociation rate of 0.15 s⁻¹. For comparison, the simulated pulling speed dependence of the unfolding force of I27 (Δx_u of 0.25 nm, spontaneous unfolding rate constant 3.3×10^{-4} s⁻¹)²¹ and rupture force of a disulfide bond in the presence of 0.25 mM hydroxide anions (Δx_u of 0.011 nm, spontaneous dissociation rate constant 0.13 s⁻¹)²⁰ are shown. In addition, simulated pulling speed dependence of the rupture force of a hypothetical bond (Δx_u of 0.05 nm and spontaneous dissociation rate constant 0.13 s⁻¹) is also shown. To facilitate the comparison, the simulated data for the disulfide is offset by 2000 pN.

corroborated that the rupture force histogram of wt-RD is indeed resulted from the rupture of the FeS₄ center.

The Distance to the Rupture Transition State of FeS₄ Is ~ 0.11 nm. The broad distribution of the rupture forces for FeS₄ is clearly beyond the experimental error in our single molecule AFM experiments, and reflects the intrinsic energy landscape underlying the mechanical activation process. The width of the distribution is related to the distance from the bound state

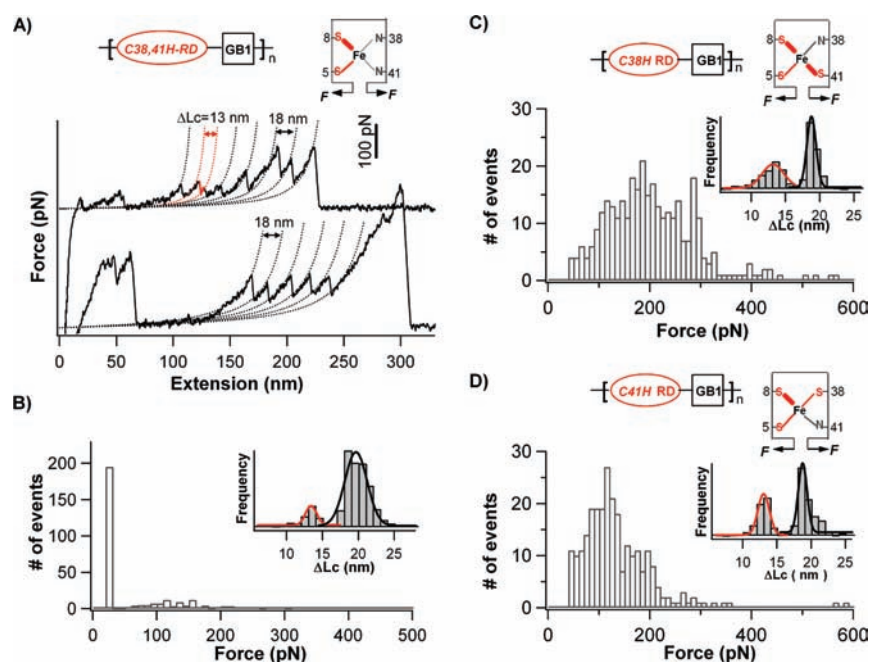


Figure 4. Dissection of the mechanical stability of the two types of Fe–thiolate bonds in the Fe(III)–S₄ center. (A) Single-molecule AFM experiments revealed that mechanical unfolding of C38,C41H-RD occurs at very low forces. The force–extension curves of (GB1-C38,41H-RD)_n are characterized by long featureless spacers followed by the unfolding events of GB1, suggesting that most C38,41H-RD unfold at low forces. Thin dotted lines are WLC fits to the data. (B) Unfolding force histogram of C38,41H-RD. The majority of C38,41H-RD occurs at forces below 20 pN, but a small population unfolds at forces around ~100 pN. Inset shows the ΔLc histograms for C38,41H-RD and GB1. It is evident that the unfolding events of C38,41H-RD are significantly fewer than that of GB1 domains (93 versus 540), consistent with the observation that the majority of C38,41H-RD unfolded at lower forces and did not show clear unfolding events with ΔLc of ~13 nm. (C) The mechanical unfolding force of Fe(III)-C38H-RD remains largely unchanged. The average unfolding force of Fe(III)-C38H-RD is 203 ± 92 pN ($n = 332$). The inset shows the ΔLc histogram of C38H-RD with an average ΔLc of 12.0 ± 1.8 nm. The number of unfolding events of C38H-RD is close to that of GB1 domains (332 versus 460). (D) Fe(III)-C41H-RD unfolds at significantly reduced forces (121 ± 74 pN ($n = 262$)). The inset shows the ΔLc histogram of C41H-RD and GB1. The average ΔLc is 12.6 ± 0.8 nm. It is of note that the number of unfolding events of C38H-RD is significantly smaller than that of GB1 domains (262 versus 472). Top panels in panels A, C, and D show the schematic structure and pulling geometry of corresponding rubredoxin mutants.

to the mechanical dissociation transition state (Δx_{u}).^{28,29} A broader distribution implies a shorter Δx_{u} . To quantitatively measure the Δx_{u} during the mechanical rupture of FeS₄, we carried out single-molecule AFM experiments at different pulling speeds (Figure 3). It is evident that the mechanical rupture force increases with the increasing of the pulling speed. On the basis of the Bell–Evans model,^{28,29} we carried out Monte Carlo simulations to reproduce the speed-dependence of the rupture force.³⁰ We found that the experimental data can be reproduced well using a Δx_{u} of 0.11 nm and spontaneous dissociation rate of 0.15 s^{-1} . Δx_{u} is about half of the bond length of the Fe(III)–thiolate bond,^{13,14} and is smaller than that for typical protein unfolding (~0.2–0.3 nm) but significantly larger than that of disulfide bond (~0.1–0.2 Å).²⁰ These differences reflect the unique nature of the Fe(III)–thiolate bonds. It is of note that data obtained here likely reflects the average properties of the FeS₄ center.

The Two Types of Different Fe(III)–S Bonds Display Different Mechanical Stability. From the geometry of the FeS₄ center, it is clear that in order to fully unfold and extend rubredoxin, at least two Fe(III)–thiolate bonds in the same CXXC chelating motif should be ruptured (Figure 1A). To prove this point, we engineered a double histidine mutant of rubredoxin C38,41H-RD, in which both Cys38 and Cys41 in the same chelating motif were substituted by histidines. Since the interactions between Fe and nitrogen atom from histidine are much

weaker than Fe(III)–thiolate bonds, we anticipated that mutation C38HC41H will significantly weaken rubredoxin. Indeed, force–extension curves of (C38,41H-RD-GB1)_n showed that the unfolding of the majority of C38,41H-RD occurred at very low forces and displayed as long featureless spacers (Figure 4A). Only a small fraction of C38,41H-RD domains showed clear unfolding events of ΔLc of ~13 nm with rupture force close to ~100 pN, leading to the observation that the number of C38,41H-RD unfolding events is only 17% of the GB1 unfolding events (93 versus 540) (Figure 4B). Mutating Cys5 and Cys8 to histidines led to similar destabilization effect (Supporting Information, Figure S4). These results clearly indicated that removing the two Fe(III)–thiolate bonds from the same CXXC chelating motif significantly weakens rubredoxin, corroborating the important roles of the two CXXC chelating motif in the mechanical stability of rubredoxin. Therefore, the two Fe–thiolate bonds in the same CXXC loop are required to provide the mechanical stability for rubredoxin.

Since the two types of Fe(III)–thiolate bonds are of different bond length,¹⁶ it is possible that they display different mechanical stability. To experimentally test this hypothesis and dissect the difference in the mechanical strength of these two types of Fe(III)–thiolate bonds, we engineered two rubredoxin mutants C38H-RD and C41H-RD. Since Fe(III)–N bond is mechanically more labile than Fe(III)–thiolate bond (Figure 4B), selectively mutating one of the two cysteines in the same CXXC motif

with histidine should allow us to determine the mechanical rupture force of the two different Fe(III)–thiolate bonds.

Stretching polyprotein (C38H-RD-GB1)_n resulted in sawtooth-like force–extension curves similar to those of wt-rubredoxin (Supporting Information, Figure S5A). The unfolding events of C38H-RD, that is, the rupture of Fe(III)–thiolate bonds, are characterized by ΔLc of 12.0 ± 1.8 nm and an average unfolding force of 203 ± 92 pN ($n = 332$) (Figure 4C). In addition, the number of unfolding event of C38H-RD is $\sim 72\%$ of that of GB1 (332 versus 460). These results suggested that the mutation C38H does not change the mechanical stability of Fe–S center significantly. Since the Fe(III)–thiolate bond formed by Cys41 remains the force-bearing bond, our results suggested that the rupture force measured on C38H-RD likely reflects the mechanical stability of the Fe(III)–S41 bond. It is of note that C38H-RD mutant is not as stable as wt rubredoxin, as we have observed that C38H-RD can lose its iron ion over time. Thus, the 28% missing events for C38H-RD are likely due to the unfolding of C38H-RD at low forces.

In contrast to C38H-RD, the unfolding events of C41H-RD were observed to occur at much lower forces of 121 ± 74 pN ($n = 262$) with ΔLc of 12.6 ± 0.8 nm (Figure 4D and Figure S5B). In addition, the number of C41H-RD unfolding events is clearly fewer than that of GB1 (262 versus 472), suggesting that some “missing” C41H-RD domains may unfold at forces below 20 pN. These results indicate that mutation C41H significantly weakens the mechanical stability of rubredoxin. Because of the mutation of C41H, the force-bearing Fe(III)–thiolate bond shifted to Fe(III)–S38 bond. Therefore, the measured rupture force for C41H-RD likely reflects the mechanical stability of Fe(III)–S38 bond. It is of note that the mechanical strength for Fe(III)–S38 and Fe(III)–S41 bonds is fittingly correlated with the bond length of these two types of Fe(III)–thiolate bonds. Thus, our results indicated that the two types of Fe(III)–thiolate bonds are not equivalent in term of their mechanical strength. The shorter Fe(III)–thiolate bonds (Fe(III)–S8 and Fe(III)–S41) are mechanically stronger than the longer Fe(III)–thiolate bonds (Fe(III)–S5 and Fe(III)–S38). To our best knowledge, this is the first direct experimental evidence that the bond strength of the two types of Fe–thiolate bonds is different. It is of note that although histidine mutation may slightly alter the structure of Fe–S center in rubredoxin, the difference in bond length of the two types of Fe(III)–thiolate bonds should remain similar: Fe–S5 and Fe–S38 bonds should be longer while Fe–S8 and Fe–S41 bonds be shorter. This trend has been observed experimentally in Cys to Ser mutants of rubredoxin in X-ray crystallographic studies.³¹ Thus, our results on histidine mutants of rubredoxin can provide a reasonable estimate of the bond strength of individual Fe–thiolate bond in rubredoxin.

DISCUSSION

Our results clearly demonstrate that the mechanical rupture force of the highly covalent Fe(III)–thiolate bonds is ~ 200 pN (with the shorter ferric–thiolate bonds being stronger than the longer ones), which is significantly lower than what one would expect for a highly covalent bond. For example, Si–Si ruptures at 2.1 nN, C–Si at 2.0 nN, and Au–S at above 2.5 nN.^{1,2,6,19} In addition, the rupture force of Fe–thiolate bond is also significantly lower than that of a disulfide bond (>1 nN), which is generally perceived as a weaker covalent bond.^{1,2,6} In contrast, the mechanical strength of ferric–thiolate bonds is more comparable

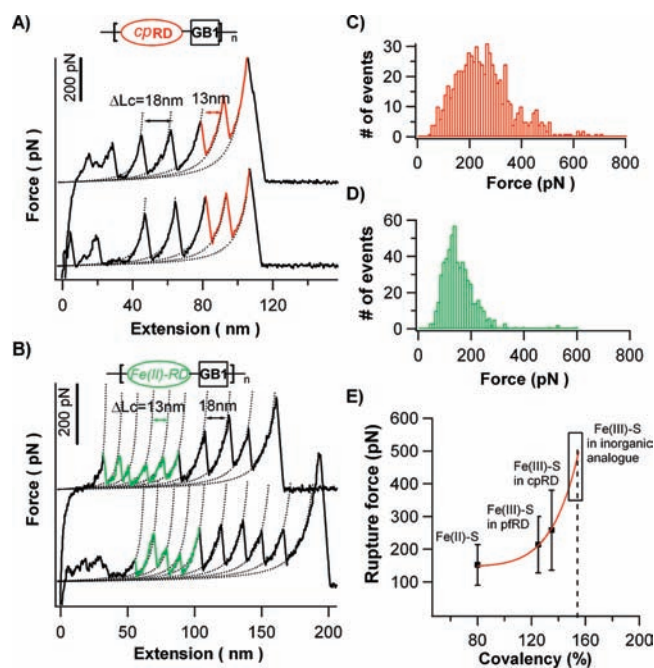


Figure 5. The rupture forces of Fe–S₄ center correlate with its covalency. (A) Typical force–extension curves of (GB1-Fe(III)-cpRD)_n. The unfolding events of cpRD tend to occur after GB1 domains have unfolded, suggesting that the rupture force of Fe–S₄ center of cpRD is higher than that of GB1. (B) Typical force–extension curves of (GB1-Fe(II)-pfRD)_n. The rupture force of Fe(II)–thiolate bonds is clearly lower than the unfolding force of GB1. Dotted lines in panels A and B correspond to the WLC fits to experimental data. (C) Histogram of the rupture force of Fe(III)–thiolate bonds in cpRD. The average rupture force is 258 ± 122 pN ($N = 686$). (D) Histogram of the rupture force of Fe(II)–thiolate bonds in pfRD. The average rupture force is 152 ± 62 pN ($n = 579$). (E) Rupture force correlates with the covalency of the Fe–thiolate bonds. The dotted line indicates the covalency of the Fe(III)–thiolate bond in [Et₄N][Fe(o-C₆H₄(CH₂S)₂)₂]. The red line is used to guide the eyes. The gray box indicates the possible range of the rupture force of Fe(III)–thiolate bonds in [Et₄N][Fe(o-C₆H₄(CH₂S)₂)₂].

to the mechanical strength of noncovalent bonds, such as hydrogen bonds. For example, the unbinding force of avidin–biotin complex is ~ 200 pN.^{3,4} The mechanical unfolding force of mechanically stable proteins ranges from ~ 50 to 300 pN, with a few proteins unfolding at more than 500 pN.^{32,33} The unfolding of such nonmetalloproteins corresponds to the rupturing of a network of noncovalent bonds, including hydrogen bonds and hydrophobic interactions. Thus, based on previous experimental results, the finding that the highly covalent ferric–thiolate bonds rupture at ~ 200 pN is unexpected and surprising. This result suggests that such Fe–thiolate bonds are mechanically labile and display features clearly distinguishing themselves from those of typical covalent bonds.

Chemical bonding reflects the degree of interactions between two atoms, and can be described by covalency, the amount of covalent mixing of their atomic orbitals.³⁴ Highly covalent nature of ferric–thiolate bonds originates from the high degree of mixing of the p orbital of sulfur atom with the d orbital of Fe atom.^{8,9,34} S–K edge XAS has been used extensively to probe the covalency of metal–thiolate bonds.¹⁰ It was discovered that the covalency of ferric–thiolate bonds depends on the chemical environment in which the ferric–thiolate bonds are located.

Because of the formation of hydrogen bonds in rubredoxin, the covalency of ferric–thiolate bond in rubredoxin is significantly lower than that of its inorganic analogues $[\text{Et}_4\text{N}][\text{Fe}(\text{o}-\text{C}_6\text{H}_4(\text{CH}_2\text{S})_2)_2]$ ($\sim 150\%$).^{15,35} These observations raise interesting questions about the relationship between covalency and mechanical strength of Fe–thiolate bonds, and the strength of the ferric–thiolate bond in the inorganic analogue. To address these issues, we measured the mechanical stability of Fe(III)–thiolate bonds in *Clostridium pasteurianum* rubredoxin (*cpRD*) and Fe(II)–thiolate bond in *pfRD*. *cpRD* is a homologue of *pfRD* with an identical FeS_4 center, but shows a higher covalency ($\sim 135\%$) than *pfRD* ($\sim 125\%$).¹⁵ Moreover, reduction of Fe(III) to Fe(II) leads to a significant decrease in the Fe–S covalency to $\sim 80\%$.³⁴ These proteins provide ideal model systems to investigate the relationship between covalency and mechanical strength.

Our single-molecule AFM experiments revealed that the rupture force of Fe(III)–thiolate bonds in *cpRD* shows a broad distribution with an average force of 258 ± 122 pN ($N = 686$) at a pulling speed of 400 nm/s (Figure 5A,C), significantly higher than that of *pfRD*. It is of note that a small number of rupture events of Fe(III)–thiolate bonds occurred even at forces between 500 and 1000 pN (Supporting Information, Figure S6). In contrast, the unfolding force for Fe(II)–thiolate is 152 ± 62 pN ($n = 579$) (Figure 5B,D), which is $\sim 30\%$ lower than the rupture force of Fe(III)–thiolate bonds in *pfRD*. It is evident that there is a positive correlation between the covalency and mechanical strength of Fe–thiolate bond: the higher covalency, the higher rupture force (Figure 5E). Clearly the mechanical strength of Fe(III)–thiolate bond in the inorganic analogue $[\text{Et}_4\text{N}][\text{Fe}(\text{o}-\text{C}_6\text{H}_4(\text{CH}_2\text{S})_2)_2]$ will be stronger than that in rubredoxin, possibly as high as 350–500 pN. Although the exact value is yet to be experimentally determined, the mechanical strength of Fe(III)–thiolate bond in $[\text{Et}_4\text{N}][\text{Fe}(\text{o}-\text{C}_6\text{H}_4(\text{CH}_2\text{S})_2)_2]$ will be still significantly lower than that of a typical covalent bond. Therefore, from a mechanical perspective, metal–thiolate bond itself is distinctly different from covalent bonds and can thus be only considered as labile highly covalent bonds. Moreover, protein environment may also play important roles in determining the mechanical strength of Fe–thiolate bonds. It is well-known that in rubredoxin the hydrogen atom of nearby amide can form backbone hydrogen bonds with the cysteine sulfur atoms. The formation of these hydrogen bonds decreases the ability of S atom binding with iron and leads to the reduction in covalency.^{9,36} Hence, the reduced mechanical stability of Fe–thiolate bond in rubredoxin is also likely due to the unique environment surrounding the FeS_4 cluster.

It is of note that the thermodynamic stability of metal–thiolate bonds depends on two major components: the first one is the covalent interaction energy, which is described by covalency, and the second one is the electrostatic interaction energy.⁹ Our single-molecule AFM results indicated that the mechanical strength of Fe–thiolate bond is correlated with its covalency, implying that the mechanical stability of metal–thiolate bond is largely determined by its covalent character and ionic character plays less important role in determining the mechanical stability of metal–thiolate bond. This implication raises the question whether the low mechanical stability of Fe(III)–thiolate bonds is due to the unique reaction pathway during the mechanical activation process of the bond.³⁷

Furthermore, our work also raises interesting questions on the mechanism of mechanical activation of Fe–thiolate bonds as well as the nature and reactivity of the broken Fe(III)–S bond.³⁸ Our preliminary results indicated that the broken Fe–S bond can

reform within rubredoxin upon relaxation of the rubredoxin chain as evidenced by the ability of rubredoxin to recover its mechanical stability. However, the mechanism of mechanical activation remains unknown. During the mechanical activation, it is possible that the breaking of Fe–thiolate bonds may be a heterolytic process involving competition with a proton, just like in traditional thermodynamic activation processes of Fe–thiolate bonds.³⁹ Similar heterolytic processes have been experimentally observed for the mechanical rupture of disulfide bonds in the presence of reducing agents^{20,26} and predicted for the mechanical rupture of polyethylene glycol.³⁸ It is also possible that the mechanical breaking of Fe–thiolate bonds is a homolytic process, as suggested for the breaking of C–Si covalent bonds.^{1,7} These two different scenarios may lead to different products (sulfhydryl versus free radical), and possibly different reactivity. This important question needs thorough mechanistic investigation by combining experiments with computational chemistry methods. Future work along this direction will be crucial to elucidate the detailed roles of covalent and ionic characters in the mechanical activation (bond rupture) process of metal–thiolate bonds as well as their reactivity after rupture. These studies will likely provide new insights into the nature of this important class of chemical bonds.

■ ASSOCIATED CONTENT

S Supporting Information. Schematics of the construction of polyprotein (Fe(III)RD-GB1)_n, the two-step unfolding mechanism of Fe(III)-RD, the description about the choice of fingerprint domains in single-molecule AFM experiments, as well as force–extension curves of polyproteins (I27-*pfRD*)_n; (C5,8H-RD-GB1)_n; (C38H-RD-GB1)_n; (C41H-RD-GB1)_n and (GB1-*cpRD*)_n. This material is available free of charge via the Internet at <http://pubs.acs.org>.

■ AUTHOR INFORMATION

Corresponding Author
Hongbin@chem.ubc.ca

■ ACKNOWLEDGMENT

We thank Prof. Pierre Kennepohl and Xuan Ding for their stimulating discussions, Dr. Yi Cao for his help with polyprotein engineering and two anonymous reviewers for their constructive suggestions. This work is supported by Natural Sciences and Engineering Research Council of Canada, Canada Research Chairs program and Canada Foundation for Innovation.

■ REFERENCES

- (1) Grandbois, M.; Beyer, M.; Rief, M.; Clausen-Schaumann, H.; Gaub, H. E. *Science* **1999**, *283* (5408), 1727–30.
- (2) Beyer, M. K.; Clausen-Schaumann, H. *Chem. Rev.* **2005**, *105* (8), 2921–48.
- (3) Florin, E. L.; Moy, V. T.; Gaub, H. E. *Science* **1994**, *264* (5157), 415–7.
- (4) Merkel, R.; Nassoy, P.; Leung, A.; Ritchie, K.; Evans, E. *Nature* **1999**, *397* (6714), 50–3.
- (5) Conti, M.; Falini, G.; Samori, B. *Angew. Chem., Int. Ed.* **2000**, *39* (1), 215–+.
- (6) Kruger, D.; Rousseau, R.; Fuchs, H.; Marx, D. *Angew. Chem., Int. Ed.* **2003**, *42* (20), 2251–3.
- (7) Beyer, M. K. *J. Chem. Phys.* **2000**, *112* (17), 7307–12.

- (8) Johnson, D. C.; Dean, D. R.; Smith, A. D.; Johnson, M. K. *Annu. Rev. Biochem.* **2005**, *74*, 247–81.
- (9) Solomon, E. I.; Gorelsky, S. I.; Dey, A. J. *Comput. Chem.* **2006**, *27* (12), 1415–28.
- (10) Solomon, E. I.; Hedman, B.; Hodgson, K. O.; Dey, A.; Szilagy, R. K. *Coord. Chem. Rev.* **2005**, *249* (1–2), 97–129.
- (11) Beinert, H. J. *Biol. Inorg. Chem.* **2000**, *5* (1), 2–15.
- (12) Holm, R. H.; Kennepohl, P.; Solomon, E. I. *Chem. Rev.* **1996**, *96* (7), 2239–14.
- (13) Blake, P. R.; Park, J. B.; Bryant, F. O.; Aono, S.; Magnuson, J. K.; Eccleston, E.; Howard, J. B.; Summers, M. F.; Adams, M. W. *Biochemistry* **1991**, *30* (45), 10885–95.
- (14) Eidsness, M. K.; Richie, K. A.; Burden, A. E.; Kurtz, D. M., Jr.; Scott, R. A. *Biochemistry* **1997**, *36* (34), 10406–13.
- (15) Rose, K.; Shadle, S. E.; Eidsness, M. K.; Kurtz, D. M.; Scott, R. A.; Hedman, B.; Hodgson, K. O.; Solomon, E. I. *J. Am. Chem. Soc.* **1998**, *120* (41), 10743–7.
- (16) Day, M. W.; Hsu, B. T.; Joshua-Tor, L.; Park, J. B.; Zhou, Z. H.; Adams, M. W.; Rees, D. C. *Protein Sci.* **1992**, *1* (11), 1494–507.
- (17) Kennepohl, P.; Solomon, E. I. *Inorg. Chem.* **2003**, *42* (3), 689–95.
- (18) Rief, M.; Gautel, M.; Oesterhelt, F.; Fernandez, J. M.; Gaub, H. E. *Science* **1997**, *276* (5315), 1109–12.
- (19) Lantz, M. A.; Hug, H. J.; Hoffmann, R.; van Schendel, P. J.; Kappenberger, P.; Martin, S.; Baratoff, A.; Guntherodt, H. J. *Science* **2001**, *291* (5513), 2580–3.
- (20) Garcia-Manyes, S.; Liang, J.; Szoszkiewicz, R.; Kuo, T. L.; Fernandez, J. M. *Nat. Chem.* **2009**, *1* (3), 236–42.
- (21) Carrion-Vazquez, M.; Oberhauser, A. F.; Fowler, S. B.; Marszalek, P. E.; Broedel, S. E.; Clarke, J.; Fernandez, J. M. *Proc. Natl. Acad. Sci. U.S.A.* **1999**, *96* (7), 3694–9.
- (22) Strop, P.; Mayo, S. L. *J. Am. Chem. Soc.* **1999**, *121* (11), 2341–5.
- (23) Cao, Y.; Li, H. *Nat. Mater.* **2007**, *6* (2), 109–14.
- (24) Sharma, D.; Perisic, O.; Peng, Q.; Cao, Y.; Lam, C.; Lu, H.; Li, H. *Proc. Natl. Acad. Sci. U.S.A.* **2007**, *104* (22), 9278–83.
- (25) Marko, J. F.; Siggia, E. D. *Macromolecules* **1995**, *28* (26), 8759–70.
- (26) Ainavarapu, S. R.; Wiita, A. P.; Dougan, L.; Uggerud, E.; Fernandez, J. M. *J. Am. Chem. Soc.* **2008**, *130* (20), 6479–87.
- (27) Wiita, A. P.; Ainavarapu, S. R.; Huang, H. H.; Fernandez, J. M. *Proc. Natl. Acad. Sci. U.S.A.* **2006**, *103* (19), 7222–7.
- (28) Bell, G. I. *Science* **1978**, *200* (4342), 618–27.
- (29) Evans, E. *Annu. Rev. Biophys. Biomol. Struct.* **2001**, *30*, 105–28.
- (30) Rief, M.; Fernandez, J. M.; Gaub, H. E. *Phys. Rev. Lett.* **1998**, *81* (21), 4764–7.
- (31) Xiao, Z. G.; Lavery, M. J.; Ayhan, M.; Scrofani, S. D. B.; Wilce, M. C. J.; Guss, J. M.; Tregloan, P. A.; George, G. N.; Wedd, A. G. *J. Am. Chem. Soc.* **1998**, *120* (17), 4135–50.
- (32) Valbuena, A.; Oroz, J.; Hervas, R.; Vera, A. M.; Rodriguez, D.; Menendez, M.; Sulkowska, J. I.; Cieplak, M.; Carrion-Vazquez, M. *Proc. Natl. Acad. Sci. U.S.A.* **2009**, *106* (33), 13791–6.
- (33) Dietz, H.; Berkemeier, F.; Bertz, M.; Rief, M. *Proc. Natl. Acad. Sci. U.S.A.* **2006**, *103* (34), 12724–8.
- (34) Glaser, T.; Hedman, B.; Hodgson, K. O.; Solomon, E. I. *Acc. Chem. Res.* **2000**, *33* (12), 859–68.
- (35) Lane, R. W.; Ibers, J. A.; Frankel, R. B.; Holm, R. H. *Proc. Natl. Acad. Sci. U.S.A.* **1975**, *72* (8), 2868–72.
- (36) Lin, I. J.; Gebel, E. B.; Machonkin, T. E.; Westler, W. M.; Markley, J. L. *Proc. Natl. Acad. Sci. U.S.A.* **2005**, *102* (41), 14581–6.
- (37) Konopka, M.; Turansky, R.; Reichert, J.; Fuchs, H.; Marx, D.; Stich, I. *Phys. Rev. Lett.* **2008**, *100* (11), 115503.
- (38) Aktah, D.; Frank, I. *J. Am. Chem. Soc.* **2002**, *124* (13), 3402–6.
- (39) Reddi, A. R.; Gibney, B. R. *Biochemistry* **2007**, *46* (12), 3745–58.